JOURNAL OF GUIDANCE, CONTROL, AND DYNAMICS
Vol. 29, No. 3, May–June 2006

Health Monitoring of a Satellite System

Robert H. Chen,* Hok K. Ng,† Jason L. Speyer,‡ and Lokeshkumar S. Guntur§
University of California, Los Angeles, Los Angeles, California 90095
and
Russell Carpenter¶
NASA Goddard Space Flight Center, Greenbelt, Maryland 20771

A health monitoring system based on analytical redundancy is developed for satellites on elliptical orbits. Analytical redundancy, which reduces the need for hardware redundancy, uses the modeled dynamic relationship between system inputs and measured system outputs to form a residual process that is used for detecting and identifying faults. First, the dynamics of the satellite including orbital mechanics and attitude dynamics is modeled as a periodic system. Then, periodic fault detection filters are designed to detect and identify the satellite's actuator and sensor faults. In addition, parity equations are constructed using the algebraic redundant relationship among actuators and sensors. Furthermore, a residual processor is designed to generate the probability of each fault by using a sequential probability test. Finally, the health monitoring system, consisting of periodic fault detection filters, parity equations, and residual processor, is evaluated in the simulation in the presence of disturbances and uncertainty.

I. Introduction

IN engineering systems, faults are always a concern. In nonautomated systems, humans often perform the fault detection and identification function. In automated systems, this function is preferred to be performed automatically. For example, satellites under automatic control demand a high degree of reliability to operate properly. If a sensor fault occurs, the controller's command will be generated using incorrect measurements. If an actuator fault occurs, the controller's command will not be applied properly to the satellite. To avoid this situation, one needs a health monitoring system capable of detecting a fault as it occurs and identifying the faulty component.

The most common approach to fault detection and identification is hardware redundancy, which is essentially the direct comparison of the outputs from multiple identical sensors using a voting scheme. To detect the fault and identify the faulty sensor, three identical sensors are required if it is assumed that only one sensor may fail. The hardware redundancy is straightforward and requires very little computation. However, it is expensive and limited by space and weight. Furthermore, it can only be applied for the sensor fault but not the actuator fault.

An alternative is analytical redundancy, which uses a detailed model of the system to compare the expected system behavior with the observed system behavior. When they differ significantly, a fault is presumed to have occurred. To detect and identify faults, one forms a residual that represents the difference between the observed and expected system variables. Nominally, the residual is nonzero only when a fault has occurred and is zero at other times. Furthermore, the residual is nonzero in a unique and a priori known direction in response to each fault. Therefore, when a nonzero residual is detected, a fault can be announced and the faulty component can be identified. Although analytical redundancy requires more computation, it does not need any redundant sensors. Furthermore, analytical redundancy can detect and identify the actuator fault in addition to the sensor fault.

One popular approach to analytical redundancy is the restricted diagonal detection filter,[1,2] which has two special cases. When every fault is detected, it becomes the Beard[3]–Jones[4] detection filter, which can be determined by algorithms in Refs. 2, 5, and 6. When only one fault is detected, it becomes the unknown input observer.[7–9] In Refs. 10–12, the unknown input observer that considers only time-invariant systems is generalized to the approximate unknown input observer that considers time-varying systems. Furthermore, the approximate unknown input observer discussed in Ref. 12 is generalized from detecting single fault to multiple faults to obtain the approximate restricted diagonal detection filter for time-varying systems.[13] Note that other filtering techniques such as Kalman filter can only be used for detecting the fault but not for identifying the fault.

Although the residual generated by the fault detection filter is nominally zero in the absence of a fault and nonzero otherwise, the residual fails to go to zero when driven by disturbances and uncertainty even in the absence of a fault. Therefore, it is sometimes difficult to determine the occurrence of a fault by simply setting a threshold for the residual. To enhance fault detection and identification, a residual processor is used to analyze the residual, which can be viewed as a pattern containing information about the presence or absence of a fault. For each fault, a hypothesis is determined according to the pattern that is unique in response to each fault. When the residual processor design is considered as a hypothesis testing problem, the residual processor could be a multiple-hypothesis Shiryayev sequential probability test (see Ref. 14). Therefore, the residual processor generates the conditional probability of each fault hypothesis rather than a binary announcement. This would allow for higher level decision making to be based on the probability.

In this paper, the fault detection filters in Refs. 12 and 13 are applied to periodic systems. For the approximate unknown input observer, the filter gain becomes periodic naturally. For the approximate restricted diagonal detection filter, an optimization problem is formulated by imposing a boundary constraint on the initial and final conditions and a numerical algorithm is proposed. This is an important extension for the approximate restricted diagonal detection filter because the periodic filter gain can be computed off-line

Presented as Paper 2004-5121 at the AIAA Guidance, Navigation, and Control Conference, Providence, RI, 16–19 August 2004; received 8 December 2004; revision received 29 June 2005; accepted for publication 22 July 2005.

*Research Engineer, Mechanical and Aerospace Engineering Department. Member AIAA.
†Graduate Student Researcher, Mechanical and Aerospace Engineering Department.
‡Mechanical and Aerospace Engineering Department; speyer@seas.ucla.edu.
§Graduate Student Researcher, Mechanical and Aerospace Engineering Department.
¶Aerospace Engineer, Flight Dynamics Analysis Branch, Code 595. Senior Member AIAA.

and stored to be used repetitively. Finally, the satellite on an elliptical orbit is modeled as a periodic system, and a health monitoring system is developed to monitor the satellite's actuators and sensors.

In Sec. II, the background of the fault detection filters in Refs. 12 and 13 and the residual processor in Ref. 14 is given. In Sec. III, both fault detection filters are applied to periodic systems. In Sec. IV, the dynamics of the satellite including orbital mechanics and attitude dynamics are modeled as a periodic system. In Sec. V, a health monitoring system is developed for the satellite, which includes periodic fault detection filters, parity equations, and residual processor. In Sec. VI, the satellite health monitoring system is evaluated in the simulation in the presence of disturbances and uncertainty.

II. Background

A. Actuator and Sensor Fault Model

Consider a linear time-varying system,

$$\dot{\boldsymbol{x}} = A(t)x + B_u(t)\boldsymbol{u} \tag{1a}$$

$$\boldsymbol{y} = C(t)\boldsymbol{x} \tag{1b}$$

where x is the state, u is the control command, and y is the measurement. The ith actuator fault can be modeled as an additive term in the state equation (1a),

$$\dot{x} = Ax + B_u u + F_a \mu_a \tag{2}$$

where the fault direction F_a is the ith column of B_u and the fault magnitude μ_a is an unknown and arbitrary scalar function of time that is zero when there is no fault.[3,5]

The ith sensor fault can be modeled as an additive term in the measurement equation (1b),

$$y = Cx + E_s \mu_s \tag{3}$$

where the fault direction E_s is a column of zeros except a one in the ith position and the fault magnitude μ_s is an unknown and arbitrary scalar function of time that is zero when there is no fault.[3,5] For the purpose of fault detection filter design, an input to the state equation that drives the measurement in the same way that μ_s does in Eq. (3) is obtained.[10] Define a new state $\bar{x} = x + f_s \mu_s$, where $E_s = C f_s$. Then, the dynamic equation of $\bar{x}$ and Eq. (3) can be written as

$$\dot{\bar{x}} = A\bar{x} + B_u u + [f_s \quad \bar{f}_s] \begin{bmatrix} \dot{\mu}_s \\ \mu_s \end{bmatrix} \tag{4a}$$

$$y = C\bar{x} \tag{4b}$$

where $\bar{f}_s = \dot{f}_s - A f_s$. Therefore, for fault detection filter design, the sensor fault is modeled as a two-dimensional additive term in the state equation as in Eq. (4). The interpretation of Eq. (4) is that f_s represents the sensor fault rate direction and $\bar{f}_s$ represents the sensor fault magnitude direction.

B. Fault Detection Filters

By using Eqs. (2) and (4), a linear time-varying system with q actuator and sensor faults can be modeled as

$$\dot{x} = Ax + B_u u + B_w w + \sum_{i=1}^{q} F_i \mu_i \tag{5a}$$

$$y = Cx + v \tag{5b}$$

where w is the process noise and v is the sensor noise. The fault direction F_i is F_a for the actuator fault as in Eq. (2) and $[f_s \quad \bar{f}_s]$ for the sensor fault as in Eq. (4). If only s of the q faults need to be detected and identified, where $1 \le s \le q$, the objective of the approximate restricted diagonal detection filter problem is to find a filter gain L for the linear filter,

$$\dot{\hat{x}} = A\hat{x} + B_u u + L(y - C\hat{x}) \tag{6a}$$

$$r = y - C\hat{x} \tag{6b}$$

where $\hat{x}$ is the estimated state such that each projected residual $\hat{H}_i r$ for $i = 1, \ldots, s$ is affected primarily by its associated target fault μ_i and minimally by its associated nuisance fault $\hat{\mu}_i = [\mu_1 \ldots \mu_{i-1} \ \mu_{i+1} \ldots \mu_q]^T$, process noise w, sensor noise v, and initial condition error $x(t_0) - \hat{x}(t_0)$. The projector $\hat{H}_i$ can be defined a priori as

$$\hat{H}_i = I - C\hat{\mathcal{T}}_i \left[(C\hat{\mathcal{T}}_i)^T C\hat{\mathcal{T}}_i \right]^{-1} (C\hat{\mathcal{T}}_i)^T \tag{7}$$

where $\hat{\mathcal{T}}_i$ spans the minimal reachable subspace of $\hat{\mu}_i$ and $C\hat{\mathcal{T}}_i = [C\boldsymbol{b}_{i,1,\delta_{i,1}} \ C\boldsymbol{b}_{i,2,\delta_{i,2}} \ldots C\boldsymbol{b}_{i,p_i,\delta_{i,p_i}}]$ (Ref. 10). The vectors $\boldsymbol{b}_{i,j,\delta_{i,j}}$, $j = 1, \ldots, p_i$, are found from the iteration defined by the Goh transformation (see Refs. 15 and 16),

$$\boldsymbol{b}_{i,j,k} = A b_{i,j,k-1} - \dot{\boldsymbol{b}}_{i,j,k-1}, \qquad \boldsymbol{b}_{i,j,0} = f_{i,j}$$

where $f_{i,j}$ is the jth column of $\hat{F}_i = [F_1 \ldots F_{i-1} \ F_{i+1} \ldots F_q]$ and $p_i = \dim \hat{F}_i$. $\delta_{i,j}$ is the smallest nonnegative integer such that $C\boldsymbol{b}_{i,j,\delta_{i,j}} \neq 0$. Note that the derivation of $\hat{H}_i$ can be included in the approximate restricted diagonal detection filter problem instead of being defined a priori to annihilate the reachable subspace of $\hat{\mu}_i$ as in Eq. (7).

To formulate the approximate restricted diagonal detection filter problem, it is assumed that $\mu_1, \ldots, \mu_q$, w and v are zero mean, white Gaussian noise with power spectral density of $Q_1, \ldots, Q_q$, Q_w, and V, respectively, and the initial state $\boldsymbol{x}(t_0)$ is a random vector with variance of P_0. It is also assumed that $\mu_1, \ldots, \mu_q$, w, and v are uncorrelated with each other and with $\boldsymbol{x}(t_0)$. By using Eqs. (5) and (6), the dynamic equation of the error, $e = x - \hat{x}$, and the residual can be written as

$$\dot{e} = (A - LC)e + \sum_{i=1}^{q} F_i \mu_i + B_w w - Lv, \qquad r = Ce + v$$

Then, the solution for the residual is

$$r(t) = C\Phi(t, t_0)\boldsymbol{e}(t_0) + C\int_{t_0}^{t} \Phi(t, \tau) \left(\sum_{i=1}^{q} F_i \mu_i + B_w w - Lv \right) \mathrm{d}\tau + v \tag{8}$$

where Φ is the transition matrix subject to

$$\frac{\mathrm{d}}{\mathrm{d}t}\Phi(t, t_0) = (A - LC)\Phi(t, t_0), \qquad \Phi(t_0, t_0) = I$$

Define

$$h_i(t) \triangleq \hat{H}_i C \int_{t_0}^{t} \Phi(t, \tau) F_i \mu_i \, \mathrm{d}\tau$$

$$\hat{h}_i(t) \triangleq \hat{H}_i C \int_{t_0}^{t} \Phi(t, \tau) \hat{F}_i \hat{\mu}_i \, \mathrm{d}\tau$$

$$\bar{h}_i(t) \triangleq \hat{H}_i C \left[\Phi(t, t_0)\boldsymbol{e}(t_0) + \int_{t_0}^{t} \Phi(t, \tau)(B_w w - Lv) \, \mathrm{d}\tau \right]$$

From solution (8), $h_i(t)$ is the transmission from μ_i to $\hat{H}_i r$, $\hat{h}_i(t)$ is the transmission from $\hat{\mu}_i$ to $\hat{H}_i r$, and $\bar{h}_i(t)$ is the transmission from w, v, and $e(t_0)$ to $\hat{H}_i r$. Note that the power spectral density of $\hat{\mu}_i$ is $\hat{Q}_i$, which is a diagonal matrix with $Q_1, \ldots, Q_{i-1}, Q_{i+1}, \ldots, Q_q$ on the diagonal line, and $\boldsymbol{e}(t_0)$ is a zero mean random vector with variance of P_0 if $\hat{\boldsymbol{x}}(t_0) = E[\boldsymbol{x}(t_0)]$. Then, the performance index for the approximate restricted diagonal detection filter problem to be minimized with respect to the filter gain is[13]

$$J = \frac{1}{t_f - t_0} \int_{t_0}^{t_f} \mathrm{tr} \left(\sum_{i=1}^{s} \left\{ \frac{1}{\gamma_i} E\left[\hat{h}_i(t) \hat{h}_i(t)^T \right] + E\left[\bar{h}_i(t) \bar{h}_i(t)^T \right] - E\left[h_i(t) h_i(t)^T \right] \right\} \right) \mathrm{d}t$$

where $E[\bullet]$ is the expectation operator and $\gamma_1, \ldots, \gamma_s$ are positive scalars. Making $\gamma_1, \ldots, \gamma_s$ small places large weightings on reducing the associated nuisance fault transmissions. Note that the power spectral densities $Q_1, \ldots, Q_q$ are considered as design parameters. Because no assumption is made on the fault magnitudes, their white noise representation is a convenience. For each projected residual, Q_i and $(1/\gamma_i)\hat{Q}_i$ represent the weightings on the associated target and nuisance fault transmissions, respectively. When Q_i is larger, the transmission from μ_i is larger. When $(1/\gamma_i)\hat{Q}_i$ is larger, the transmission from $\hat{\mu}_i$ is smaller. Similarly, when Q_w, V, and P_0 are larger, the transmission from the process noise, sensor noise, and initial condition error respectively, is smaller.

After some manipulations, the optimization problem for the approximate restricted diagonal detection filter becomes[13]

$$\min_L \frac{1}{t_f - t_0} \int_{t_0}^{t_f} \mathrm{tr}\left[\sum_{i=1}^{s} \hat{H}_i C W_i C^T \hat{H}_i \right] \mathrm{d}t \tag{9}$$

subject to

$$\dot{W}_i = (A - LC)W_i + W_i(A - LC)^T + \left(L - P_i C^T V^{-1}\right) V \left(L - P_i C^T V^{-1}\right)^T, \qquad W_i(t_0) = 0 \tag{10}$$

where

$$\dot{P}_i = A P_i + P_i A^T - P_i C^T V^{-1} C P_i + (1/\gamma_i)\hat{F}_i \hat{Q}_i \hat{F}_i^T - F_i Q_i F_i^T + B_w Q_w B_w^T, \qquad P_i(t_0) = P_0 \tag{11}$$

for $i = 1, \ldots, s$. Note that Eq. (11) is solved independently of L. By using continuously differentiable matrix Lagrange multipliers K_i to adjoin the constraint to the cost, the first-order necessary conditions imply that the optimal solution for L and the dynamics of K_i are[17]

$$L^* = \left(\sum_{i=1}^{s} K_i \right)^{-1} \left[\sum_{i=1}^{s} K_i (P_i + W_i) \right] C^T V^{-1} \tag{12}$$

satisfying Eq. (10) and

$$-\dot{K}_i = K_i(A - LC) + (A - LC)^T K_i + C^T \hat{H}_i C, \qquad K_i(t_f) = 0 \tag{13}$$

where $i = 1, \ldots, s$. Therefore, the process of deriving the filter gain requires the solution to a two-point boundary-value problem that includes a set of Lyapunov equations (10) and (13), coupled by Eq. (12). An alternative approach to derive the filter gain is to solve Eq. (9) numerically by using the steepest descent method. However, the global minimum cannot be guaranteed because Eq. (9) may not be convex. Note that the filter gain has to be computed off-line because of the two-point boundary-value problem.

When $s = q$, the approximate restricted diagonal detection filter becomes the approximate Beard–Jones detection filter. When $s = 1$, the approximate restricted diagonal detection filter becomes the approximate unknown input observer. For the approximate unknown input observer problem that detects the fault μ_i and blocks the fault $\hat{\mu}_i$, the minimization problem (9) reduces to[12]

$$\min_L \frac{1}{t_f - t_0} \int_{t_0}^{t_f} \mathrm{tr}\left[\hat{H}_i C W_i C^T \hat{H}_i \right] \mathrm{d}t$$

subject to Eq. (10). By inspection, the optimal filter gain is

$$L^* = P_i C^T V^{-1} \tag{14}$$

using the solution to Eq. (11). Note that the filter gain can be computed online because Eq. (11) is integrated forward. Also note that s approximate unknown input observers are needed to monitor all s faults.

C. Residual Processor

The residual processing problem here is considered as a hypothesis testing problem that can be solved by using the multiple-hypothesis Shiryayev sequential probability test (MHSSPT) (see Ref. 14). MHSSPT is a generalized result from Ref. 18 that solves the change detection problem based on the results of Ref. 19 and by using a dynamic programming formulation. For a certain criterion of optimality, MHSSPT detects and isolates a change in hypothesis in the conditionally independent measurement sequence in minimum time. In the dynamic programming formulation, the measurement cost, the cost of false alarm, and the cost of miss alarm are considered. MHSSPT is shown to be optimal in the infinite time case.

To apply the hypothesis testing problem to the fault detection and identification problem, the measurement sequence is the residual generated by the fault detection filter. For each fault, a hypothesis $\mathcal{H}_i$ is defined according to the pattern of the residual that is unique in response to each fault. Also, a null hypothesis $\mathcal{H}_0$ is defined for the no-fault case. Then, the propagation equation for the posterior probability of each hypothesis conditioned on the measurement sequence is[14]

$$P(\theta_i \le t_{k+1} | X_{k+1}) = \frac{P(\theta_i \le t_{k+1} | X_k) f_i(\boldsymbol{x}_{k+1})}{\sum_{j=0}^{s} P(\theta_j \le t_{k+1} | X_k) f_j(\boldsymbol{x}_{k+1})} \tag{15a}$$

$$P(\theta_i \le t_{k+1} | X_k) = P(\theta_i \le t_k | X_k) + \tilde{p}_i [1 - P(\theta_i \le t_k | X_k)] \tag{15b}$$

$$P(\theta_0 \le t_{k+1} | X_k) = \prod_{j=1}^{s} [1 - P(\theta_j \le t_{k+1} | X_k)] \tag{15c}$$

where θ_i is the time of transition to hypothesis $\mathcal{H}_i$, $\boldsymbol{x}_k$ is the measurement vector at time t_k, X_k is the measurement sequence up to t_k, $f_i(\boldsymbol{x}_k)$ is the probability density function of $\boldsymbol{x}_k$ given hypothesis $\mathcal{H}_i$, and $\tilde{p}_i$ is the a priori probability of transition to hypothesis $\mathcal{H}_i$ from t_k to t_{k+1}. This recursive algorithm allows the posterior probability of each hypothesis to be computed online and plays a central role in the dynamic programming analysis.

The propagation equation (15) is derived using Bayes rule under three assumptions. First, the measurement sequence X_k is conditionally independent or equivalently $P(\theta_i \le t_k | X_k) = P(\theta_i \le t_k | \boldsymbol{x}_k)$ $P(\theta_i \le t_k | \boldsymbol{x}_{k-1}), \ldots, P(\theta_i \le t_k | \boldsymbol{x}_1)$. In the application to the fault detection and identification problem, however, the measurement sequence might be time correlated.

Second, the probability density function $f_i(x)$ is assumed known for all hypotheses. In practice, however, the magnitude of the fault is typically unknown, which means incomplete information about the mean of the distribution. To deal with this problem, if one of the parameters of $f_i(x)$, denoted as α, is unknown and assumed to follow its own distribution, that is, a probability density function $\psi_\alpha(x)$ defined over Ω, then the conditional probability density function becomes[14]

$$f_i(x) = \int_\Omega f_i(x|\eta) \psi_\alpha(\eta)\, \mathrm{d}\eta$$

For example, assume that the measurement sequence has Gaussian distributions under different hypotheses with known variances and unknown means that have uniform distributions as $x \sim \mathcal{N}(m_i, \Lambda_i)$ and $m_i \sim \mathrm{Unif}[b_i, b_i + 2m_i^*]$. Then, the conditional probability density function can be written as

$$f_i(x) = \left(1 \Big/ 4^n \prod_{j=1}^{n} m_{ij}^* \right) \left[\mathrm{erf}\left\{ \frac{1}{\sqrt{2}} \Lambda_i^{-\frac{1}{2}} (x - b_i) \right\} - \mathrm{erf}\left\{ \frac{1}{\sqrt{2}} \Lambda_i^{-\frac{1}{2}} (x - b_i - 2m_i^*) \right\} \right] \tag{16}$$

where $m_i^* = [m_{i1}^* \ldots m_{in}^*]^T$.

Third, the a priori probability of transition $\tilde{p}_i$ is assumed known for all hypotheses and constant for all stages. Note that the analysis remains the same even if it is stage dependent. Also, the initial condition $P(\theta_i \le t_0)$ is assumed known for all hypotheses. In practice,

both parameters are considered as design parameters. In general, a smaller $\tilde{p}_i$ is chosen when the measurement sequence is noisier.

III. Periodic Fault Detection Filter

In this section, the fault detection filters in Refs. 12 and 13 are applied to periodic systems. Consider a linear periodic system with q faults similar to Eq. (5) except $A(t+T)=A(t)$, $B_u(t+T)=B_u(t)$, $C(t+T)=C(t)$, $B_w(t+T)=B_w(t)$, $F_i(t+T)=F_i(t)$, and T is the period. Under the assumptions of controllability and observability, the Riccati matrix P_i in Eq. (11) converges to a unique periodic solution (see Refs. 20 and 21). Therefore, the filter gain (14) of the approximate unknown input observer becomes periodic naturally.

For the approximate restricted diagonal detection filter problem, a boundary constraint on the initial and final conditions is imposed on the minimization problem (9),

$$\min_{L,W_1(t_0),\ldots,W_s(t_0)} J=\min_{L,W_i(t_0),\ldots,W_s(t_0)}\int_{t_0}^{t_0+T}\operatorname{tr}\left[\sum_{i=1}^{s}\hat{H}_i C W_i C^T\hat{H}_i\right]\mathrm{d}t \tag{17}$$

subject to

$$\dot{W}_i=(A-LC)W_i+W_i(A-LC)^T+\left(L-P_iC^TV^{-1}\right)V\left(L-P_iC^TV^{-1}\right)^T \tag{18a}$$

$$\Psi_i=W_i(t_0+T)-W_i(t_0)=0 \tag{18b}$$

for $i=1,\ldots,s$. In Sec. III.A, the first-order necessary condition for the minimization problem (17) is derived. In Sec. III.B, the minimization problem is transformed from the matrix form to the vector form because the matrix boundary constraint (18b) cannot be included in the formulation of the numerical algorithm proposed in Sec. III.C. Also, the part of the minimization problem in the vector form that is associated with the symmetric part of the minimization problem in the matrix form is reduced. In Sec. III.C, the steepest descent numerical algorithm is proposed to solve the minimization problem in its reduced-order vector form.

A. First-Order Necessary Condition

By taking the first-order variation of Eqs. (17) and (18),

$$\delta J=\int_{t_0}^{t_0+T}\operatorname{tr}\left[\sum_{i=1}^{s}C^T\hat{H}_iC\delta W_i\right]\mathrm{d}t \tag{19a}$$

$$\delta\dot{W}_i=(A-LC)\delta W_i+\delta W_i(A-LC)^T+\left(LV-P_iC^T-W_iC^T\right)\delta L^T+\delta L\left(LV-P_iC^T-W_iC^T\right)^T \tag{19b}$$

$$\delta\Psi_i=\delta W_i(t_0+T)-\delta W_i(t_0) \tag{19c}$$

By using continuously differentiable matrix Lagrange multipliers K_i and matrix Lagrange multipliers ν_i to adjoin the constraints (19b) and (19c) to the cost (19a), respectively,

$$\delta J=\int_{t_0}^{t_0+T}\operatorname{tr}\left\{\sum_{i=1}^{s}\left[\dot{K}_i+K_i(A-LC)+(A-LC)^TK_i+C^T\hat{H}_iC\right]\delta W_i+\sum_{i=1}^{s}\left[2K_i\left(LV-P_iC^T-W_iC^T\right)\right]\delta L^T\right\}\mathrm{d}t-\sum_{i=1}^{s}[K_i(t_0+T)-\nu_i]\delta W_i(t_0+T)+\sum_{i=1}^{s}[K_i(t_0)-\nu_i]\delta W_i(t_0)$$

Therefore, the first-order necessary condition for the minimization problem (17) is

$$L^*=\left(\sum_{i=1}^{s}K_i\right)^{-1}\left[\sum_{i=1}^{s}K_i(P_i+W_i)\right]C^TV^{-1} \tag{20}$$

satisfying Eq. (18) and

$$-\dot{K}_i=K_i(A-LC)+(A-LC)^TK_i+C^T\hat{H}_iC \tag{21a}$$

$$0=K_i(t_0+T)-K_i(t_0) \tag{21b}$$

where $i=1,\ldots,s$. The process of deriving the periodic filter gain of the approximate restricted diagonal detection filter requires the solution to a two-point boundary-value problem that includes a set of Lyapunov equations (18) and (21), coupled by Eq. (20). An alternative approach to derive the periodic filter gain is to solve Eq. (17) numerically by using the steepest descent method. In Sec. III.B, Eq. (19) is transformed from the matrix form to the vector form because the matrix boundary constraint (19c) cannot be included in the formulation of the numerical algorithm proposed in Sec. III.C.

B. Transformation from Matrix Form to Vector Form

Let

$$\delta W_i=\begin{bmatrix}\delta w_{i1} & \delta w_{i2} & \cdots & \delta w_{in}\end{bmatrix}$$

$$\delta\Psi_i=\begin{bmatrix}\delta\psi_{i1} & \delta\psi_{i2} & \cdots & \delta\psi_{in}\end{bmatrix}$$

where $\delta w_{i1},\ldots,\delta w_{in}$ are the column vectors of δW_i and $\delta\psi_{i1},\ldots,\delta\psi_{in}$ are the column vectors of $\delta\Psi_i$. Then, Eq. (19c) can be written as

$$\delta\psi_i=\delta w_i(t_0+T)-\delta w_i(t_0) \tag{22}$$

where

$$\delta w_i=\begin{bmatrix}\delta w_{i1}\\ \delta w_{i2}\\ \vdots\\ \delta w_{in}\end{bmatrix},\qquad \delta\psi_i=\begin{bmatrix}\delta\psi_{i1}\\ \delta\psi_{i2}\\ \vdots\\ \delta\psi_{in}\end{bmatrix}$$

Let

$$C^T\hat{H}_iC=\begin{bmatrix}h_{i1}^T\\ h_{i2}^T\\ \vdots\\ h_{in}^T\end{bmatrix}$$

where $h_{i1}^T,\ldots,h_{in}^T$ are the row vectors of $C^T\hat{H}_iC$. Then, Eq. (19a) can be written as

$$\delta J=\int_{t_0}^{t_0+T}\left(\sum_{i=1}^{s}\sum_{j=1}^{n}h_{ij}^T\delta w_{ij}\right)\mathrm{d}t=\int_{t_0}^{t_0+T}\left(\sum_{i=1}^{s}h_i^T\delta w_i\right)\mathrm{d}t \tag{23}$$

where

$$h_i^T=\begin{bmatrix}h_{i1}^T & h_{i2}^T & \cdots & h_{in}^T\end{bmatrix}$$

Let

$$\delta L=\begin{bmatrix}\delta l_1^T\\ \delta l_2^T\\ \vdots\\ \delta l_n^T\end{bmatrix},\qquad A-LC=\begin{bmatrix}\boldsymbol{a}_1^T\\ \boldsymbol{a}_2^T\\ \vdots\\ \boldsymbol{a}_n^T\end{bmatrix}$$

$$LV-P_iC^T-W_iC^T=\begin{bmatrix}\boldsymbol{v}_{i1}^T\\ \boldsymbol{v}_{i2}^T\\ \vdots\\ \boldsymbol{v}_{in}\end{bmatrix}$$

where $\delta l_1^T,\ldots,\delta l_n^T$ are the row vectors of δL, $\boldsymbol{a}_1^T,\ldots,\boldsymbol{a}_n^T$ are the row vectors of $A-LC$, and $\boldsymbol{v}_{i1}^T,\ldots,\boldsymbol{v}_{in}^T$ are the row vectors of

$LV - P_iC^T - W_iC^T$. Because δW_i is symmetric, $\delta w_{i1}^T \ldots \delta w_{in}^T$ are the row vectors of δW_i. Then, from Eq. (19b),

$$\delta \dot{w}_{ij} = \begin{bmatrix} \boldsymbol{a}_1^T \delta w_{ij} \\ \boldsymbol{a}_2^T \delta w_{ij} \\ \vdots \\ \boldsymbol{a}_n^T \delta w_{ij} \end{bmatrix} + \begin{bmatrix} \delta w_{i1}^T \boldsymbol{a}_j \\ \delta w_{i2}^T \boldsymbol{a}_j \\ \vdots \\ \delta w_{in}^T \boldsymbol{a}_j \end{bmatrix} + \begin{bmatrix} \boldsymbol{v}_{i1}^T \delta l_j \\ \boldsymbol{v}_{i2}^T \delta l_j \\ \vdots \\ \boldsymbol{v}_{in}^T \delta l_j \end{bmatrix} + \begin{bmatrix} \delta l_1^T \boldsymbol{v}_{ij} \\ \delta l_2^T \boldsymbol{v}_{ij} \\ \vdots \\ \delta l_n^T \boldsymbol{v}_{ij} \end{bmatrix}$$

$$= \bar{A}_j \delta w_i + \bar{B}_{ij} \delta l$$

for $j = 1, \ldots, n$, where

$$\bar{A}_j = \begin{bmatrix} \boldsymbol{a}_j^T & 0 & \cdots & 0 \\ 0 & \boldsymbol{a}_j^T & 0 & \vdots \\ \vdots & 0 & \ddots & 0 \\ 0 & \cdots & 0 & a_j^T \end{bmatrix} + \begin{bmatrix} 0 & \cdots & 0 & \boldsymbol{a}_1^T & 0 & \cdots & 0 \\ 0 & \cdots & 0 & \boldsymbol{a}_2^T & 0 & \cdots & 0 \\ \vdots & \ddots & \vdots & \vdots & \vdots & \ddots & \vdots \\ 0 & \cdots & 0 & \boldsymbol{a}_n^T & 0 & \cdots & 0 \end{bmatrix}$$

$$\bar{B}_{ij} = \begin{bmatrix} \boldsymbol{v}_{ij}^T & 0 & \cdots & 0 \\ 0 & \boldsymbol{v}_{ij}^T & 0 & \vdots \\ \vdots & 0 & \ddots & 0 \\ 0 & \cdots & 0 & \boldsymbol{v}_{ij}^T \end{bmatrix} + \begin{bmatrix} 0 & \cdots & 0 & \boldsymbol{v}_{i1}^T & 0 & \cdots & 0 \\ 0 & \cdots & 0 & \boldsymbol{v}_{i2}^T & 0 & \cdots & 0 \\ \vdots & \ddots & \vdots & \vdots & \vdots & \ddots & \vdots \\ 0 & \cdots & 0 & \boldsymbol{v}_{in}^T & 0 & \cdots & 0 \end{bmatrix}$$

$$\delta l = \begin{bmatrix} \delta l_1 \\ \delta l_2 \\ \vdots \\ \delta l_n \end{bmatrix}$$

The nonzero column block vectors in the second matrices on the right-hand side of $\bar{A}_j$ and $\bar{B}_{ij}$ are at the jth block column. The dimensions of the zero block elements on the right-hand side of $\bar{A}_j$ and $\bar{B}_{ij}$ are 1 by n and 1 by m, respectively, where n is the number of the states and m is the number of the measurements. Then, Eq. (19b) can be written as

$$\delta \dot{w}_i = \bar{A} \delta w_i + \bar{B}_i \delta l \tag{24}$$

where

$$\bar{A} = \begin{bmatrix} \bar{A}_1 \\ \bar{A}_2 \\ \vdots \\ \bar{A}_n \end{bmatrix}, \qquad \bar{B}_i = \begin{bmatrix} \bar{B}_{i1} \\ \bar{B}_{i2} \\ \vdots \\ \bar{B}_{in} \end{bmatrix}$$

Now the vector form of Eq. (19) is obtained as Eqs. (23), (24) and (22).

Because δW_i is symmetric, δw_i has $n(n-1)/2$ redundant elements and the dimension of δw_i can be reduced by $n(n-1)/2$. Let the jth and kth elements of δw_i be one pair of the symmetric part of δW_i. The kth element of δw_i can be removed as follows. For Eq. (22), the kth row is removed. For Eq. (23), the kth column of h_i^T is first added to the jth column of h_i^T and then the kth column of h_i^T is removed. For Eq. (24), the kth rows of $\bar{A}$ and $\bar{B}_i$ are first removed and then the kth column of $\bar{A}$ is added to the jth column of $\bar{A}$ before the kth column of $\bar{A}$ is removed. This procedure will be repeated to remove all $n(n-1)/2$ redundant elements of δw_i.

C. Steepest Descent Numerical Algorithm

In this section, the steepest descent numerical algorithm is proposed to solve the minimization problem (17) using the reduced-order form of (23), (24), and (22). By using continuously differentiable Langrange multipliers λ_i to adjoin the constraint (24) to the cost (23),

$$\delta J = \int_{t_0}^{t_0+T} \sum_{i=1}^{s} \left[\left(\dot{\lambda}_i^T + \lambda_i^T \bar{A} + h_i^T \right) \delta w_i + \lambda_i^T \bar{B}_i \delta l \right] \mathrm{d}t$$

$$- \sum_{i=1}^{s} \lambda_i^T (t_0+T) \delta w_i (t_0+T) + \sum_{i=1}^{s} \lambda_i^T (t_0) \delta w_i (t_0)$$

Let

$$\dot{\lambda}_i = -\bar{A}^T \lambda_i - h_i, \qquad \lambda_i (t_0+T) = 0 \tag{25}$$

Then,

$$\delta J = \int_{t_0}^{t_0+T} \left(\sum_{i=1}^{s} \lambda_i^T \bar{B}_i \right) \delta l \, \mathrm{d}t + \sum_{i=1}^{s} \lambda_i^T (t_0) \delta w_i (t_0) \tag{26}$$

From Eq. (24)

$$\delta w_i (t_0+T) = \Phi (t_0+T, t_0) \delta w_i (t_0) + \int_{t_0}^{t_0+T} \Phi (t_0+T, t) \bar{B}_i \delta l \, \mathrm{d}t$$

where

$$\dot{\Phi} (t_0+T, t) = -\Phi (t_0+T, t) \bar{A}, \qquad \Phi (t_0+T, t_0+T) = I$$

Then, Eq. (22) becomes

$$\delta \psi_i = [\Phi (t_0+T, t_0) - I] \delta w_i (t_0) + \int_{t_0}^{t_0+T} \Phi (t_0+T, t) \bar{B}_i \delta l \, \mathrm{d}t \tag{27}$$

By using Langrange multipliers ν_i to adjoin the constraint (27) to the cost (26),

$$\delta J + \sum_{i=1}^{s} \nu_i^T \delta \psi_i = \int_{t_0}^{t_0+T} \sum_{i=1}^{s} \left\{ \left[\lambda_i^T + \nu_i^T \Phi (t_0+T, t) \right] \bar{B}_i \right\} \delta l \, \mathrm{d}t$$

$$+ \sum_{i=1}^{s} \left\{ \lambda_i^T (t_0) + \nu_i^T [\Phi (t_0+T, t_0) - I] \right\} \delta w_i (t_0)$$

For the steepest descent numerical algorithm, δl and $\delta w_i (t_0)$ are chosen as

$$\delta l = -\epsilon \sum_{i=1}^{s} \left\{ \left[\lambda_i^T + \nu_i^T \Phi (t_0+T, t) \right] \bar{B}_i \right\}^T \tag{28a}$$

$$\delta w_i (t_0) = -\epsilon \left\{ \lambda_i^T (t_0) + \nu_i^T [\Phi (t_0+T, t_0) - I] \right\}^T \tag{28b}$$

where ϵ is a positive scalar to be chosen arbitrarily. By substituting Eq. (28) into Eq. (27),

$$[\Phi (t_0+T, t_0) - I] \left[\Phi^T (t_0+T, t_0) - I \right] \nu_i$$

$$+ \sum_{j=1}^{s} \left[\int_{t_0}^{t_0+T} \Phi (t_0+T, t) \bar{B}_i \bar{B}_j^T \Phi^T (t_0+T, t) \, \mathrm{d}t \right] \nu_j$$

$$= -\frac{\delta \psi_i}{\epsilon} - [\Phi (t_0+T, t_0) - I] \lambda_i (t_0)$$

$$- \sum_{j=1}^{s} \int_{t_0}^{t_0+T} \Phi (t_0+T, t) \bar{B}_i \bar{B}_j^T \lambda_j \, \mathrm{d}t$$

where $\delta \psi_i$ can be chosen arbitrarily. This can be written as

$$\begin{bmatrix} m_{11} & m_{12} & \cdots & m_{1s} \\ m_{12}^T & m_{22} & \cdots & m_{2s} \\ \vdots & \vdots & \ddots & \vdots \\ m_{1s}^T & m_{2s}^T & \cdots & m_{ss} \end{bmatrix} \begin{bmatrix} \nu_1 \\ \nu_2 \\ \vdots \\ \nu_s \end{bmatrix} = \begin{bmatrix} z_1 \\ z_2 \\ \vdots \\ z_s \end{bmatrix} \tag{29}$$

where

$$m_{ii} = [\Phi(t_0+T,t_0)-I]\left[\Phi^T(t_0+T,t_0)-I\right] + \int_{t_0}^{t_0+T} \Phi(t_0+T,t)\bar{B}_i\bar{B}_i^T\Phi^T(t_0+T,t)\,\mathrm{d}t$$

$$m_{ij} = \int_{t_0}^{t_0+T} \Phi(t_0+T,t)\bar{B}_i\bar{B}_j^T\Phi^T(t_0+T,t)\,\mathrm{d}t$$

$$z_i = -\frac{\delta\psi_i}{\epsilon} - [\Phi(t_0+T,t_0)-I]\lambda_i(t_0) - \sum_{j=1}^{s}\int_{t_0}^{t_0+T}\Phi(t_0+T,t)\bar{B}_i\bar{B}_j^T\lambda_j\,\mathrm{d}t$$

Therefore, Eqs. (28) and (29) form the updates of the steepest descent numerical algorithm for determining the periodic filter gain of the approximate restricted diagonal detection filter. The steepest descent algorithm is an iterative process starting with an initial guess of L and $W_i(t_0)$ and then repeat the following steps.

1) Integrate Eq. (18) forward.

2) Convert the minimization problem from the matrix form into the vector form.

3) Integrate Eq. (25) backward.

4) Update l and $w_i(t_0)$ using Eqs. (28) and (29).

5) Convert l into L and $w_i(t_0)$ into $W_i(t_0)$.

This procedure is repeated until δl and $\delta w_i(t_0)$ are smaller than some predetermined values. This is an important extension for the approximate restricted diagonal detection filter because the periodic filter gain can be computed off-line and stored to be used repetitively. Note that if the matrix form of the first-order variation (19) is used instead of the vector form, the matrix Langrange multipliers, used to adjoin the matrix boundary constraint (19c) to the cost, cannot be solved analytically as Eq. (29). Instead, they will have to be solved numerically. Also note that if the full-order form of Eqs. (23), (24), and (22) is used instead of the reduced-order form, the Langrange multipliers determined by Eq. (29) will not be symmetric nor will Eq. (28b) be symmetric when they are converted into the matrix form. Therefore, the reduced-order form of Eqs. (23), (24), and (22) is necessary for the formulation of the steepest descent numerical algorithm.

Remark 1: Instead of solving the minimization problem (17) with boundary constraint (18b), the periodic approximate restricted diagonal detection filter can also be determined by solving Eq. (17) without constraint (18b) over multiple periods instead of single period. The update of the steepest descent numerical algorithm for this problem becomes

$$\delta l = -\epsilon\sum_{i=1}^{s}\bar{B}_i^T\lambda_i \tag{30}$$

using Eq. (18a) with $W_i(t_0)=0$ and Eq. (25) with $\lambda_i(t_f)=0$, where t_f depends on the number of periods chosen. The optimal filter gain obtained for this problem is over multiple periods and not periodic. However, the part of the optimal filter gain associated with the period in the middle of the multiple periods is expected to be periodic.

IV. Satellite Model

In this section, an Earth pointing satellite, which keeps one face of the satellite pointed to the Earth all of the time, is modeled as a periodic system. The actuators considered are three thrusters. The sensors considered are a star sensor, a horizon sensor, a sun sensor, a loosely coupled global positioning system (GPS), and an inertial measurement unit, which has three gyros and three accelerometers.

A. Dynamics of Satellite

The equations of motion associated with the orbital mechanics of the satellite are

$$\ddot{\boldsymbol{r}} + (\mu/\|\boldsymbol{r}\|^3)r - C_B^I u_a = 0 \tag{31}$$

where $\boldsymbol{r} = [r_x \;\; r_y \;\; r_z]^T$ is the position vector of the satellite in Earth-centered inertial (ECI) reference frame; $u_a = [u_{a_x} \;\; u_{a_y} \;\; u_{a_z}]^T$ is the specific thrust in satellite reference frame, where each component is generated by the one of the three thrusters; C_B^I is the transformation from the satellite reference frame to ECI reference frame, and μ is the Earth gravitational constant.

The attitude dynamics of the satellite is modeled for the nominal operation of the satellite where the three attitude angles $\Theta = [\phi \;\; \theta \;\; \psi]^T$ are defined as the angles between the nadir reference frame (i.e., the system of coordinates that maintain their orientation relative to the Earth as the satellite moves on its orbit) and satellite reference frame. (See the figure on page 29 of Ref. 22). The relationship between these two reference frames is

$$w_{IB}^B = w_{NB}^B + C_N^B w_{IN}^N \tag{32}$$

where w_{IB}^B is the angular velocity of satellite reference frame with respect to ECI reference frame expressed in the satellite reference frame, w_{NB}^B is the angular velocity of satellite reference frame with respect to the nadir reference frame expressed in the satellite reference frame, w_{IN}^N is the angular velocity of nadir reference frame with respect to ECI reference frame expressed in the nadir reference frame, and C_N^B is the transformation from the nadir reference frame to satellite reference frame. Assume that the attitude angles are small, which is the case for an Earth pointing satellite. Then, w_{NB}^B can be approximated by $\dot{\Theta}$ to the first order and from Eq. (32),

$$\dot{\Theta} = -C_N^B w_{IN}^N + w_{IB}^B \tag{33}$$

This can be used as the equations of motion associated with the attitude dynamics of the satellite given that w_{IB}^B is measured by the gyros. Note that the thrusters are only used for orbit control and attitude control is done by other means such as reaction wheels, which are not in the scope of this paper.

By combining Eqs. (31) and (33), the equations of motion of the satellite are

$$\frac{\mathrm{d}}{\mathrm{d}t}\begin{bmatrix} r \\ \dot{r} \\ \Theta \end{bmatrix} = \begin{bmatrix} \dot{r} \\ -\dfrac{\mu}{\|r\|^3}r + C_N^I C_B^N u_a \\ -C_N^B w_{IN}^N + w_{IB}^B \end{bmatrix} \tag{34}$$

where C_B^N is the transformation from the satellite reference frame to nadir reference frame and C_N^I is the transformation from the nadir reference frame to ECI reference frame. Note that w_{IN}^N and C_N^I are functions of r and $\dot{r}$ and C_B^N is a function of Θ. Also note that u_a is the control input generated by the thrusters and w_{IB}^B is the measured input obtained by using the gyros.

B. Measurement Model

1. Star Sensor

Star sensor measures the azimuth ϕ_{star} and elevation λ_{star} of a star in the star sensor reference frame and provides attitude information of the satellite by comparing the measured star coordinate to the a priori known star coordinate in the star catalog.[22] The measured unit vector in the direction of the star in the star sensor reference frame is

$$\hat{\boldsymbol{s}} = [-\sin\phi_{\text{star}}\cos\lambda_{\text{star}} \quad \cos\phi_{\text{star}}\cos\lambda_{\text{star}} \quad -\sin\lambda_{\text{star}}]^T$$

which can be related to the unit vector $\boldsymbol{s}$ in the direction of the star in ECI reference frame from the star catalog by

$$\hat{\boldsymbol{s}} = C_N^B C_I^N \boldsymbol{s}$$

In this paper, the star is chosen to be 15 deg of right ascension and 10 deg of declination in ECI reference frame, although different stars can be chosen over the course of the orbit.

2. Horizon Sensor

Horizon sensor measures the angle between the satellite to Earth's two horizons by scanning the Earth with the scanner's line of sight sweeping from one horizon to the other and multiplying the time it takes to scan by the angular rate of the scanner rotation.[23] Horizon sensor usually operates with two synchronized scanners to scan upper and lower sides of the Earth that have equal distance to the center of the Earth. When there is no roll rotation, the times that it takes for the two scanners to scan the Earth are equal. When there is any roll rotation, one scanner will take longer to scan the Earth than the other scanner. The difference of the time $\triangle t$ can be related to the roll angle ϕ by

$$v\triangle t = 4\phi\frac{2\|r\|^2 + R_e^2}{2\|r\|^2 - R_e^2}$$

where v is the angular rate of the scanner rotation and R_e is the radius of the Earth. When there is no pitch rotation, the satellite's x axis is perpendicular to the plane containing the two lines of sight at the middle of the scanning process. When there is any pitch rotation, the angle γ_h between the satellite's x axis and the plane containing the two lines of sight at the middle of the scanning process is

$$\gamma_h = \pi/2 - \theta$$

where θ is the pitch angle.

3. Other Sensors

Sun sensor is similar to the star sensor except that it measures the azimuth ϕ_{sun} and elevation λ_{sun} of the sun.[22] For the loosely coupled GPS, the measurement is the position of the satellite in ECI reference frame.

$$y_{\text{gps}} = [r_x \quad r_y \quad r_z]^T$$

For the inertial measurement unit, there are three gyros and three accelerometers. The three gyros measure the angular velocity of satellite reference frame with respect to ECI reference frame,

$$y_{\text{gyro}} = w_{IB}^B$$

The three accelerometers can only measure nongravitational forces such as thrust, air drag, and solar radiation pressure. Because thrust is dominant over other small perturbations, it is assumed that the accelerometers only measure the specific thrust,

$$y_a = \begin{bmatrix} y_{a_x} & y_{a_y} & y_{a_z} \end{bmatrix}^T = \begin{bmatrix} u_{a_x} & u_{a_y} & u_{a_z} \end{bmatrix}^T \tag{35}$$

C. Linearized Satellite Model

Because the periodic fault detection filter design requires a linear model, the equations of motion (34) and the measurement model in Sec. IV.B are linearized around a Keplerian reference orbit with zero attitude angles. The Keplerian reference orbit is chosen with semimajor axis of 6998.12 km, eccentricity of 0.01, inclination of 5 deg with respect to the Earth's equatorial plane, right ascension of the ascending node of 20 deg, and argument of perigee of 15 deg. On the reference orbit, the nominal u_a is zero and the nominal w_{IB}^B is equal to w_{IN}^N. Let the state x and input u be

$$x = \begin{bmatrix} r \\ \dot{r} \\ \Theta \end{bmatrix}, \qquad u = \begin{bmatrix} u_a \\ y_{\text{gyro}} \end{bmatrix}$$

Denote the nominal state as x_0 and nominal input as u_0.

The linearized equations of motion of the satellite is

$$\delta\dot{x} = A\delta x + B\delta u \tag{36}$$

where A and B are the partial derivatives of the equations of motion (34) with respect to the state and input, respectively, being evaluated at x_0 and u_0. Because some elements in the A and B matrices are too complex to take the partial derivative analytically, A and B are obtained numerically by using the central difference method. Because there are sensor noise in the gyros and uncertainty between the control commands and the control inputs generated by the thrusters, a process noise w is added to Eq. (36) and the linearized equations of motion become

$$\delta\dot{x} = A\delta x + B\delta u + Bw \tag{37}$$

Similarly, the linearized measurement equation is obtained by linearizing the measurement model of the star sensor measurement $y_{\text{star}} = [\phi_{\text{star}} \quad \lambda_{\text{star}}]^T$, horizon sensor measurement $y_h = [v\triangle t \quad \gamma_h]^T$, sun sensor measurement $y_{\text{sun}} = [\phi_{\text{sun}} \quad \lambda_{\text{sun}}]^T$, and GPS measurement y_{gps},

$$\delta y = \begin{bmatrix} \delta y_{\text{star}}^T & \delta y_h^T & \delta y_{\text{sun}}^T & \delta y_{\text{gps}}^T \end{bmatrix}^T = C\delta x \tag{38}$$

where C is the partial derivative of the measurement model with respect to the state being evaluated at x_0. Because some elements in the C matrix are too complex to take the partial derivative analytically, C is obtained numerically by the using central difference method. Furthermore, sensor noise v is added to Eq. (38), and the linearized measurement equation becomes

$$\delta y = C\delta x + v \tag{39}$$

V. Development of Satellite Health Monitoring System

In this section, a health monitoring system consisting of periodic fault detection filters, parity equations, and residual processor, as in Fig. 1, is developed to monitor the satellite's actuators and sensors. Because the GPS receiver can have its own health monitoring system,[24] it does not need to be included in the proposed health monitoring system.

A. Periodic Fault Detection Filter Design

In this section, two periodic multiple-fault detection filters, that is, periodic approximate restricted diagonal detection filter or periodic approximate Beard–Jones detection filter, are designed to monitor the three thrusters, star sensor, horizon sensor, sun sensor, and three gyros. Because the three accelerometers measure only the control inputs but not the states, they are monitored by the parity equations in Sec. V.B. To design the periodic multiple-fault detection filter, the fault direction of each fault is obtained first. The fault directions for the three thruster faults and three gyro faults are the first and last three columns of the B matrix in Eq. (37), respectively. The fault directions for the star sensor, horizon sensor, and sun sensor faults cannot be formed because the C matrix in Eq. (39) loses rank and there exists no f_s in Eq. (4). Therefore, a periodic multiple-fault detection filter is designed for the three thrusters and three gyros using Eqs. (37) and (39), whereas another periodic multiple-fault detection filter is designed for the star sensor, horizon sensor, and sun sensor using Eq. (37) and a reduced-order measurement model that is full-rank and includes the GPS measurement and only one

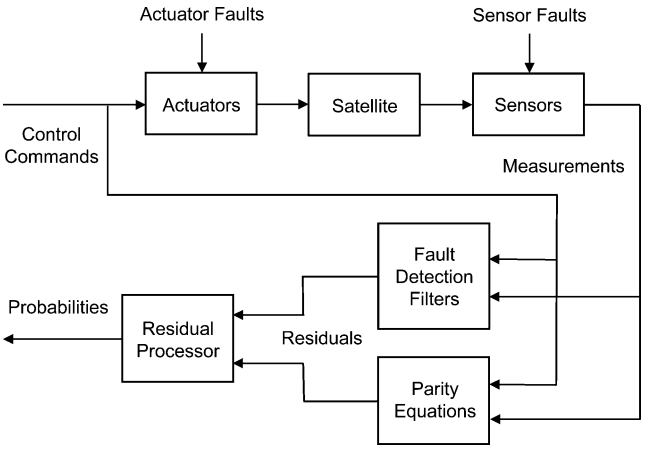

Fig. 1 Structure of satellite health monitoring system.

component from the measurement of each of the star sensor, horizon sensor, and sun sensor. Here ϕ_{star}, γ_h, and λ_{sun} are chosen because they provide a better rank condition for the reduced-order measurement matrix over the entire period than other possible combinations.

1. Three Thrusters and Three Gyros

Because this fault group has six faults and all of them need to be detected and identified, $q = s = 6$ in Eqs. (5) and (17), and the first periodic multiple-fault detection filter is a periodic approximate Beard–Jones detection filter. For each fault, its associated target fault F_i, associated nuisance fault $\hat{F}_i$, projector $\hat{H}_i$, and periodic Riccati matrix P_i are obtained first. The associated target fault is the fault itself. The associated nuisance fault is the other five faults. The projector is formed by using Eq. (7). The periodic Riccati matrix is obtained by integrating Eq. (11) with design weightings chosen as $Q_i = 0.99$, $\gamma = 10^{-2}$, $\hat{Q}_i = I$, $V = I$, and $Q_w = I$. Note that V and Q_w are considered as design parameters instead of noise variances. Also note that V and Q_w could be different for each Riccati equation because they represent the weightings of the transmission from the sensor and process noises to different projected residuals.

Now the periodic multiple-fault detection filter for the three thrusters and three gyros can be obtained by using the steepest descent numerical algorithm in Sec. III.C. When using a numerical algorithm to solve an optimization problem, the initial guess of the solution plays an important role in whether the algorithm will converge to the correct solution or not. Because the three thruster and three gyro faults do not have complementary subspace, that is, the detection spaces of these six faults span the entire state space, a good initial guess for the filter gain can be formed as[13]

$$L = \left(\sum_{i=1}^{s} H_i\right)^{-1} \left(\sum_{i=1}^{s} H_i P_i\right) C^T V^{-1} \tag{40}$$

where

$$H_i = I - \hat{T}_i \left(\hat{T}_i^T \hat{T}_i\right)^{-1} \hat{T}_i^T$$

and $\hat{T}_i = [b_{i,1,0} \ldots b_{i,1,\delta_{i,1}} \; b_{i,2,0} \ldots b_{i,2,\delta_{i,2}} \ldots b_{i,p_i,0} \ldots b_{i,p_i,\delta_{i,p_i}}]$. The initial guess for $W_i(t_0)$ can be obtained by integrating Eq. (18a) with $W_i(t_0) = 0$ and Eq. (40) until W_i becomes periodic.

As explained in Remark 1, the minimization problem (17) can be solved with boundary constraint for single period or without boundary constraint for multiple periods. The second approach is used here with five periods. Therefore, the steepest descent numerical algorithm used here is an iterative process starting with an initial guess of L and then repeating the following steps.

1) Integrate Eq. (18a) forward with $W_i(t_0) = 0$.

2) Convert the minimization problem from the matrix form into the vector form.

3) Integrate Eq. (25) backward with $\lambda_i(t_0 + 5T) = 0$.

4) Update l using Eq. (30).

5) Convert l into L.

Note that the optimal filter gain obtained is over five periods and is not periodic. However, the part of the optimal filter gain associated with the third period is periodic and is used as the solution for the periodic multiple-fault detection filter.

Remark 2: The six periodic single-fault detection filters, that is, periodic approximate unknown input observer, for the three thrusters and three gyros can be obtained by using Eq. (14). Although the periodic single-fault detection filters can be derived more easily, the computation requirement for implementation is six times greater than using just one periodic multiple-fault detection filter.

2. Star Sensor, Horizon Sensor, and Sun Sensor

To design the second periodic multiple-fault detection filter, the fault directions of the star sensor, horizon sensor, and sun sensor faults are obtained first by using Eq. (4) and

$$f_s = \bar{C}^T (\bar{C}\bar{C}^T)^{-1} E_s$$

$$\dot{f}_s = \dot{\bar{C}}^T (\bar{C}\bar{C}^T)^{-1} E_s - \bar{C}^T (\bar{C}\bar{C}^T)^{-1} (\dot{\bar{C}}\bar{C}^T + \bar{C}\dot{\bar{C}}^T)(\bar{C}\bar{C}^T)^{-1} E_s$$

where $\bar{C}$ is the reduced-order measurement matrix that includes the GPS measurement, ϕ_{star}, γ_h, and λ_{sun}. Note that $\bar{f}_s$, the fault directions representing the fault magnitudes, are very small and about three orders smaller than f_s, the fault directions representing the fault rates. This indicates that if the faults are low frequency, it will be difficult to detect the faults because both $\bar{f}_s$ and the fault rate are near zero. For example, if the associated target fault is a bias, the corresponding projected residual will become small after a while even though the associated target fault still exists. However, if the associated target fault is a ramp, the corresponding projected residual will stay large because the fault rate is nonzero. Physically, this is because the star sensor, horizon sensor, and sun sensor measure functions of mainly the angles that are the integration of the angular rates. If the dynamics of the angular rates is not (or is weakly) affected by the angles, then integrating angular rates will not be able to verify whether the angles are off by a bias. On the other hand, because $\bar{f}_s$ are very small, the periodic multiple-fault detection filter may be designed using only f_s. The advantage is that the periodic multiple-fault detection filter can detect and identify more faults in one filter because the dimension of the fault is reduced. The disadvantage is that the projected residual may be a little more sensitive to its associated nuisance fault because the fault magnitude direction of the associated nuisance fault is not blocked. However, the fault magnitude direction of the associated nuisance fault may be included in the process noise to improve the blocking of the associated nuisance fault.

Next, for each fault, its associated target fault F_i, associated nuisance fault $\hat{F}_i$, projector $\hat{H}_i$, and periodic Riccati matrix P_i are obtained. The associated target fault is the fault itself. The associated nuisance fault is the other two faults. For the star sensor fault, the periodic Riccati matrix is obtained with design weightings chosen as $Q_i = 1$, $\gamma = 10^{-2}$, $\hat{Q}_i = I$, and $V = I$, and Q_w is a diagonal matrix with 10^3, 0.1, 10^3, 10^3, 10^{-3}, and 10^3 on the diagonal line. For the horizon sensor fault, the periodic Riccati matrix is obtained with design weightings chosen as $Q_i = 0.85$, $\gamma = 10^{-2}$, $\hat{Q}_i = I$, and $V = I$, and $Q_w = I$. For the sun sensor fault, the periodic Riccati matrix is obtained with design weightings chosen as $Q_i = 0.1$, $\gamma = 10^{-2}$, $\hat{Q}_i = I$, and $V = I$, and Q_w is a diagonal matrix with 10^4, 10^4, 10^4, 1, 10^2, and 10^4 on the diagonal line. Note that there is a process noise assumed in Eq. (37) to model the uncertainty between the control commands and the control inputs generated by the thrusters and the sensor noise of the gyros.

Now, the periodic multiple-fault detection filter for the star sensor, horizon sensor, and sun sensor can be obtained by using the steepest descent numerical algorithm in Sec. III.C. Because the star sensor, horizon sensor, and sun sensor faults have a complementary subspace, a initial guess cannot be formed because Eq. (40) is not applicable. To deal with this problem, arbitrary fault directions are added to fill up the state space so that the three sensor faults and the additional fault directions together do not have a complementary subspace. For example, if the additional fault directions are chosen as the three thruster faults, there will be no complementary subspace. Then, Riccati matrices are obtained for the additional fault directions, and the Riccati matrices for the three sensor faults are obtained again because they are different from those derived earlier because the associated nuisance faults now include five faults instead of two faults. By using these six Riccati matrices, the initial guess for the filter gain is determined from Eq. (40). Note that the Riccati matrices for the additional fault directions are used only for forming the initial guess and not for solving the minimization problem (17).

Finally, the minimization problem (17) can be formulated in two ways. First, if the original Riccati matrices for the three sensor faults are used, then $q = s = 3$ and the periodic multiple-fault detection filter is a periodic approximate Beard–Jones detection filter. Second, if the new Riccati matrices for the three sensor faults are used, then $q = 6$ and $s = 3$, and the periodic multiple-fault detection filter is a periodic approximate restricted diagonal detection filter. The first formulation is used here, and the minimization problem (17) is solved without boundary constraint using the same steepest descent numerical algorithm given in the preceding section. Note that

the optimal filter gain obtained is over five periods and is not periodic. However, the part of the optimal filter gain associated with the third period is periodic and is used as the solution for the periodic multiple-fault detection filter. Also note that the three periodic single-fault detection filters for the star sensor, horizon sensor, and sun sensor can be obtained by using Eq. (14).

B. Parity Equation Design

For the satellite modelled in Sec. IV.C, in addition to the dynamic relationship among the actuators and sensors that is used to design periodic fault detection filters, there exists algebraic redundant relationship among the actuators and sensors that can be used to construct parity equations. In this section, six parity equations are formed.

From Eq. (35), the relationship between the thrusters and accelerometers is used to construct the first three parity equations,

$$r_1 = y_{a_x} - u_{a_x} \tag{41a}$$

$$r_2 = y_{a_y} - u_{a_y} \tag{41b}$$

$$r_3 = y_{a_z} - u_{a_z} \tag{41c}$$

For each residual, it is zero when there is no fault and becomes nonzero when its corresponding thruster fault or corresponding accelerometer fault occurs. Therefore, each parity equation can detect that a fault occurs but cannot distinguish between a thruster fault and an accelerometer fault. However, because the thruster fault can be detected by the first periodic multiple-fault detection filter, the thruster and accelerometer faults can be detected and identified by examining the residuals of the parity equations along with the projected residuals of the first periodic multiple-fault detection filter assuming that the thruster and accelerometer faults do not occur at the same time.

Note that the projected residual of the filter becomes large gradually when the thruster fault occurs because of the filter dynamics, whereas the residual of the parity equation becomes large immediately when the thruster or accelerometer fault occurs. Therefore, during the first few seconds when the thruster fault occurs, the pattern of the residuals matches the pattern of the accelerometer fault case instead of the thruster fault case. This could create a false identification in the residual processor. To avoid this problem, a first-order lag with time constant of $10/3$ s is added to the parity equation (41) such that the residual of the parity equation becomes large gradually similar to the projected residual of the filter. Therefore, the first three parity equations are

$$\dot{r}_1 = -0.3r_1 + 0.3\left(y_{a_x} - u_{a_x}\right)$$

$$\dot{r}_2 = -0.3r_2 + 0.3\left(y_{a_y} - u_{a_y}\right)$$

$$\dot{r}_3 = -0.3r_3 + 0.3\left(y_{a_z} - u_{a_z}\right)$$

Note that it is expected that it will take a few seconds for the residual processor to detect and identify the fault because the residuals become large gradually when the fault occurs. However, a separate residual processor can be designed to process only the residual of the parity equation without the lag, that is, Eq. (41). Then, the second residual processor can detect the fault immediately after the occurrence of a fault, whereas the first residual processor can identify the fault a few seconds later.

Because three singular values of the C matrix in Eq. (39) are much smaller than the other six singular values over the entire period, there exists algebraic redundant relationship among the star sensor, horizon sensor, sun sensor, and GPS that can be used to construct three parity equations. To construct parity equations that are not sensitive to certain faults, three reduced-order measurement models, $\delta y_r = C_r \delta x$, are formed without using one of the star sensor, horizon sensor, and sun sensor, respectively. For each reduced-order measurement matrix C_r, there is one singular value that is much smaller than the other six singular values over the entire period. Therefore, one parity equation can be formed for each reduced-order measurement model as

$$r = z^T \delta y_r$$

where z is the left singular vector of C_r associated with the smallest singular value and $z^T C_r \approx 0$. Because each reduced-order measurement model excludes one sensor, each of the three parity equations will not be sensitive to one of the three sensor faults. Therefore, these three parity equations can detect and identify the star sensor, horizon sensor, and sun sensor faults assuming that only one fault occurs at a time. When the residuals of these three parity equations are examined along with the residual of the second periodic multiple-fault detection filter, the fault detection and identification for the star sensor, horizon sensor, and sun sensor are enhanced.

C. Residual Processor Design

In this section, a residual processor is designed to generate the probability of each of the actuator and sensor faults by processing the residuals generated by two periodic multiple-fault detection filters and six parity equations. For the first periodic multiple-fault detection filter, there are six projected residuals and each projected residual is a 9 by 1 vector. For the second periodic multiple-fault detection filter, there are three projected residuals and each projected residual is a 6 by 1 vector. For each parity equation, there is one residual, which is a scaler. Therefore, the measurement sequence for the residual processor is a 78 by 1 vector, which leads to intensive computation. To alleviate this problem, the norm of the residual is used instead of the residual itself. Then, the measurement sequence for the residual processor becomes a 15 by 1 vector. The other advantage of processing the norm of the residual is that only one hypothesis is needed for each fault. Otherwise, two hypotheses are needed, where one is for the positive fault magnitude and the other is for the negative fault magnitude.

There are 13 hypotheses for the residual processor: $\mathcal{H}_0$ is the null hypothesis, that is, no fault; $\mathcal{H}_1$ is the first thruster-fault hypothesis; $\mathcal{H}_2$ is the second thruster-fault hypothesis; $\mathcal{H}_3$ is the third thruster-fault hypothesis; $\mathcal{H}_4$ is the first gyro-fault hypothesis; $\mathcal{H}_5$ is the second gyro-fault hypothesis; $\mathcal{H}_6$ is the third gyro-fault hypothesis; $\mathcal{H}_7$ is the star sensor-fault hypothesis; $\mathcal{H}_8$ is the horizon sensor-fault hypothesis; $\mathcal{H}_9$ is the sun sensor-fault hypothesis; $\mathcal{H}_{10}$ is the first accelerometer-fault hypothesis; $\mathcal{H}_{11}$ is the second accelerometer-fault hypothesis; and $\mathcal{H}_{12}$ is the third accelerometer-fault hypothesis. Under each hypothesis, the measurement sequence is assumed Gaussian distributed with a known variance and an unknown mean that is uniformly distributed. Therefore, the conditional probability density function of each hypothesis can be defined by Eq. (16). The mean and variance are determined from the simulation. For the null hypothesis, the mean is chosen to be uniformly distributed between 0 and 0.5 because the norms of all 15 residuals are less than 0.5 when there is no fault. For each of the other hypotheses, the mean is chosen by using the range of the norms of the residuals when different magnitudes of the fault are imposed in the simulation. For all hypotheses, the variances are calculated from the norms of the residuals. Note that the measurement sequence can be assumed as distributions other than the Gaussian distribution. Finally, the a priori probabilities of transition and the initial conditions $P(\theta_i \le t_0)$, are considered as design parameters. The a priori probabilities of transition for hypotheses $\mathcal{H}_1, \ldots, \mathcal{H}_{12}$ are chosen as 10^{-8}. The initial conditions $P(\theta_i \le t_0)$ for hypotheses $\mathcal{H}_1, \ldots, \mathcal{H}_{12}$ are chosen as 0.001.

VI. Evaluation of Satellite Health Monitoring System

In this section, the satellite health monitoring system is evaluated in the simulation in the presence of disturbances and uncertainty. Instead of the reference orbit, the satellite travels on another Keplerian orbit with the same orbital elements except that the semimajor axis is 20 km larger. Realistic sensor noise is imposed on the sensors as white Gaussian noise with standard deviation of 4.8346×10^{-5} rad for the star sensor, 8.5×10^{-3} and 8.7266×10^{-4} rad for the horizon sensor, 7.2606×10^{-5} rad for the sun sensor, 1 m for the

GPS, 0.0005 rad/s for the three gyros, and 0.1 m/s^2 for the three accelerometers.[22] To evaluate the performance of the satellite health monitoring system, a bias fault of 1 m/s^2 is imposed on each of the three thrusters separately at the 2000th second. Note that the satellite will only deviate from the desired trajectory by 8 m in 4 s for the given thruster fault. Also, a bias fault of 10 times larger than the standard deviation of the sensor noise is imposed on the star sensor, horizon sensor, sun sensor, three gyros, and three accelerometers separately at the 2000th second. In Sec. VI.A, the implementation of the satellite health monitoring system is discussed. In Sec. VI.B, the performance of the satellite health monitoring system is shown.

A. Implementation of Satellite Health Monitoring System

The two periodic multiple-fault detection filters, the six parity equations, and the residual processor are implemented with measurements updated at 10 Hz. The parameters of the periodic multiple-fault detection filters are stored as a table with time of the reference orbit as the index over one period. When the satellite is at time point t, the filter parameters and nominal measurement on the reference orbit are obtained first. Then, the residual is obtained by using the current state estimate propagated at previous time point $t-0.1$ and the measurement variation, which is the difference between the current measurement and the nominal measurement. Finally, the state estimate for next time point $t+0.1$ is obtained. To obtain the filter parameters and nominal measurement at time point t, the point on the reference orbit that is closest to the position of the satellite measured by the GPS at time point $t-2$ is obtained. Then, by projecting 2 s ahead of this point along the reference orbit, the filter parameters and nominal measurement at the new point are used as the filter parameters and nominal measurement at time point t. The position of the satellite at time point $t-2$ is used instead of at time point t because the position of the satellite measured by the GPS at time point t might be incorrect due to possible GPS fault, whereas the position of the satellite measured by the GPS at time point $t-2$ is already verified by a separate health monitoring system built in the GPS receiver.[24] It is assumed here that a GPS fault can be detected within 2 s. The implementation of parity equations is similar, and the implementation of residual processor is straightforward.

B. Simulation Results

In this section, the performance of the satellite health monitoring system is shown when each of the three thruster-, three gyro-, three accelerometer-, star sensor-, horizon sensor-, and sun sensor-faults occurs. When one of the three thruster-, three gyro-, and three accelerometer-faults occurs, only the residuals of the first periodic multiple-fault detection filter and the first three parity equations are shown because these faults are not included in the design of the second periodic multiple-fault detection filter and the last three parity equations whose residuals will respond to these faults arbitrarily. Similarly, when one of the star sensor-, horizon sensor-, and sun sensor-faults occurs, only the residuals of the second periodic multiple-fault detection filter and the last three parity equations are shown. Note that the residual processor uses the residuals of both periodic multiple-fault detection filters and all six parity equations no matter which fault occurs.

When the first thruster fault occurs, the norms of the residuals and probabilities are as shown in Figs. 2 and 3, respectively. Note that the norms of the projected residuals of the first periodic multiple-fault detection filter are scaled such that they become one when their associated target faults occur and when the satellite travels on the reference orbit without any disturbances and uncertainty. Figure 2 shows that the residuals respond to the fault in accordance with their design. Figure 3 shows that the residual processor announces the thruster fault correctly in about 4 s. When the second and third thruster faults occur, the residuals and probabilities respond in a similar way and, therefore, are not shown here. For these two thruster faults, the residual processor also announces the fault correctly in about 4 s.

When the first gyro fault occurs, the norms of the residuals and probabilities are as shown in Figs. 4 and 5, respectively. Figure 4

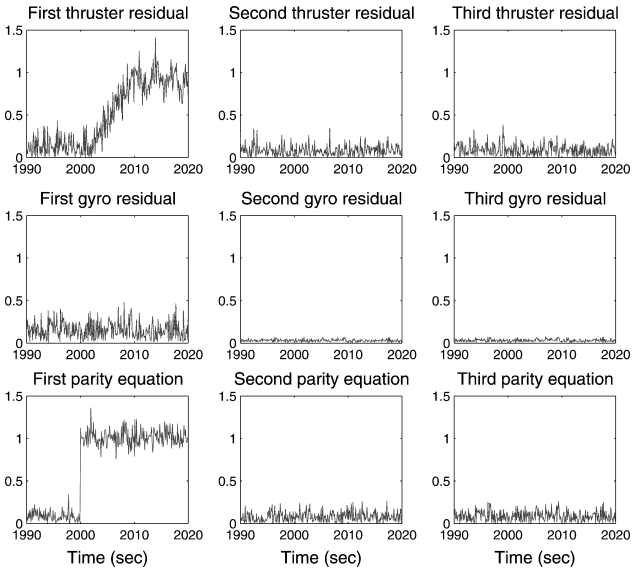

Fig. 2 Residuals when first thruster fault occurs.

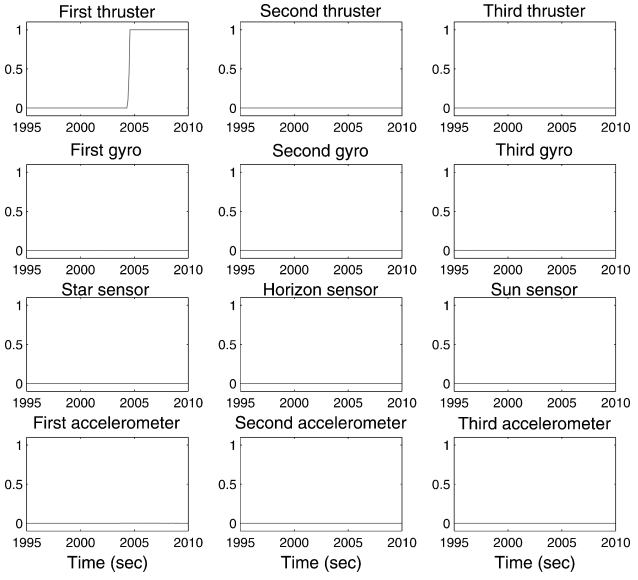

Fig. 3 Probabilities when first thruster fault occurs.

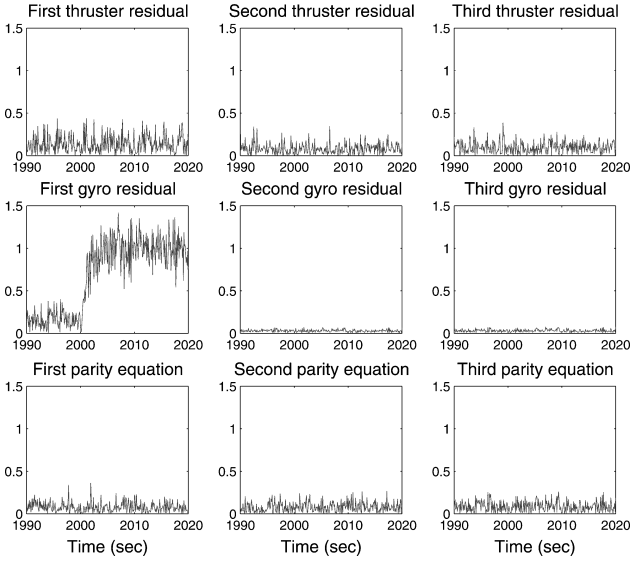

Fig. 4 Residuals when first gyro fault occurs.

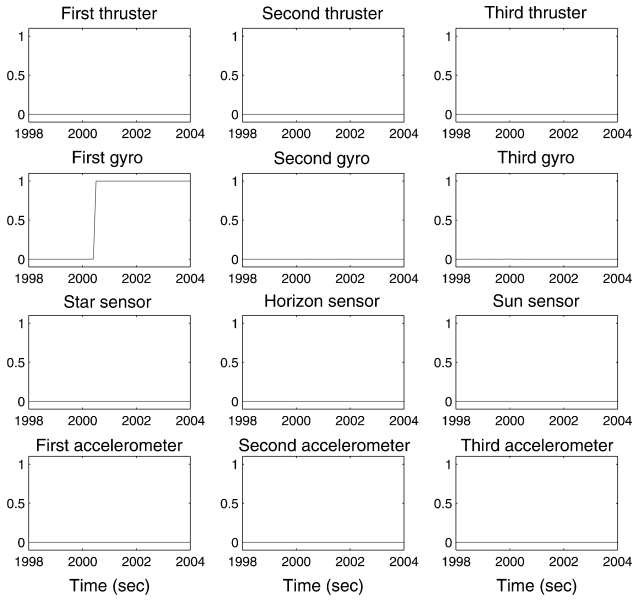

Fig. 5 Probabilities when first gyro fault occurs.

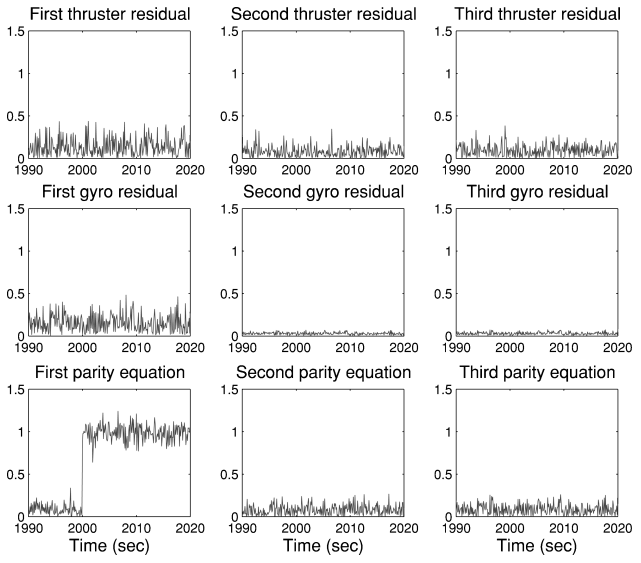

Fig. 6 Residuals when first accelerometer fault occurs.

shows that the residuals respond to the fault in accordance to the way they are designed to. Figure 5 shows that the residual processor announces the gyro fault correctly in about $\frac{1}{2}$ s. When the second and third gyro faults occur, the residuals and probabilities respond in a similar way and, therefore, are not shown here. For these two gyro faults, the residual processor announces the fault correctly in about $1\frac{1}{2}$ s. Figures 2 and 4 show that the first periodic multiple-fault detection filter can detect and identify the three thruster and three gyro faults very well because, when each of these six faults occurs, only the corresponding projected residual becomes large while the other five projected residuals remain small.

When the first accelerometer fault occurs, the residuals and probabilities are as shown in Figs. 6 and 7, respectively. Figure 6 shows that the residuals respond to the fault in accordance to the way they are designed to. Figure 7 shows that the residual processor announces the accelerometer fault correctly in about 4 s. When the second and third accelerometer faults occur, the residuals and probabilities respond in a similar way and, therefore, are not shown here. For these two accelerometer faults, the residual processor also announces the fault correctly in about 4 s.

When the star sensor fault occurs, the residuals and probabilities are as shown in Figs. 8 and 9, respectively. When the horizon

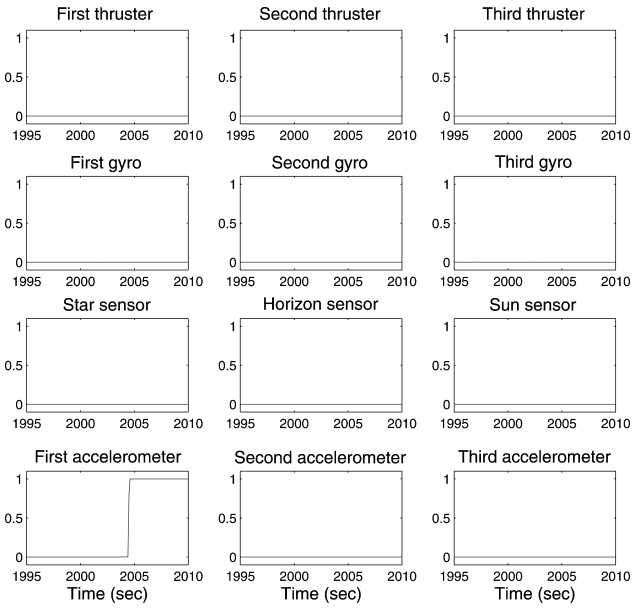

Fig. 7 Probabilities when first accelerometer fault occurs.

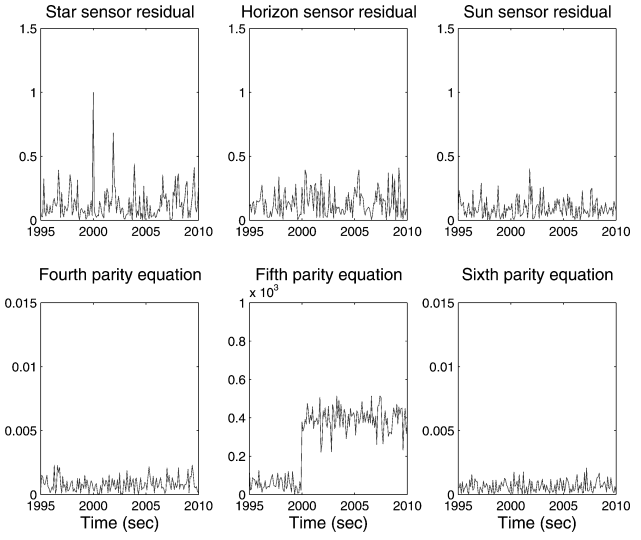

Fig. 8 Residuals when star sensor fault occurs.

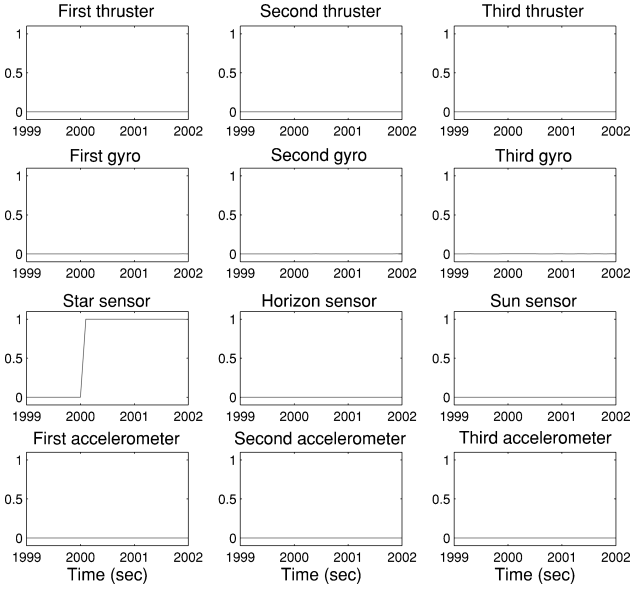

Fig. 9 Probabilities when star sensor fault occurs.

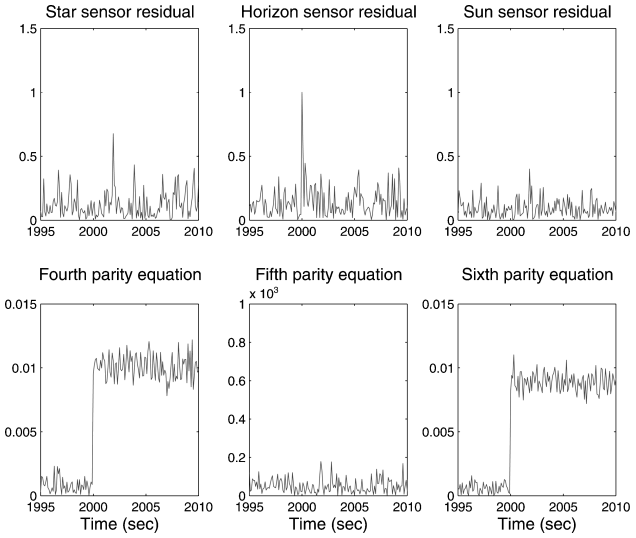

Fig. 10 Residuals when horizon sensor fault occurs.

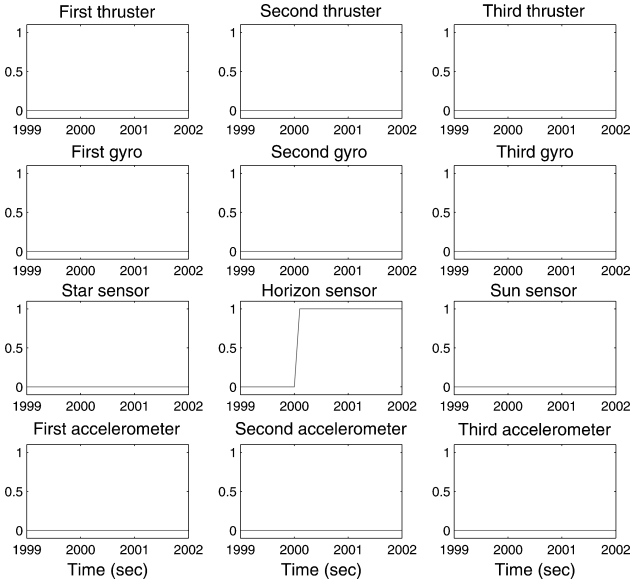

Fig. 11 Probabilities when horizon sensor fault occurs.

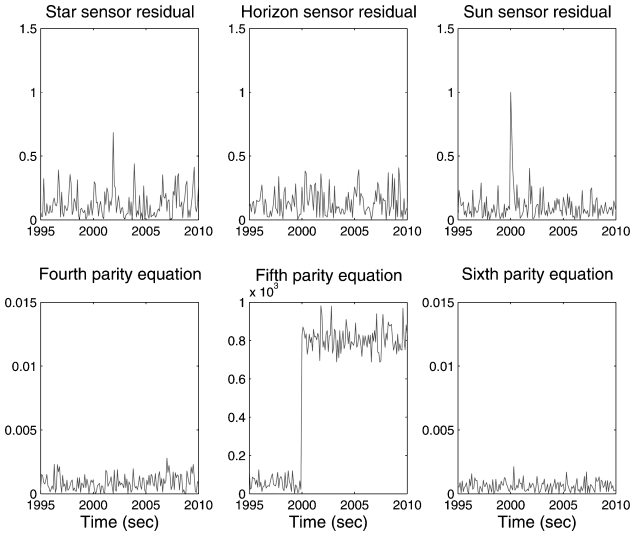

Fig. 12 Residuals when sun sensor fault occurs.

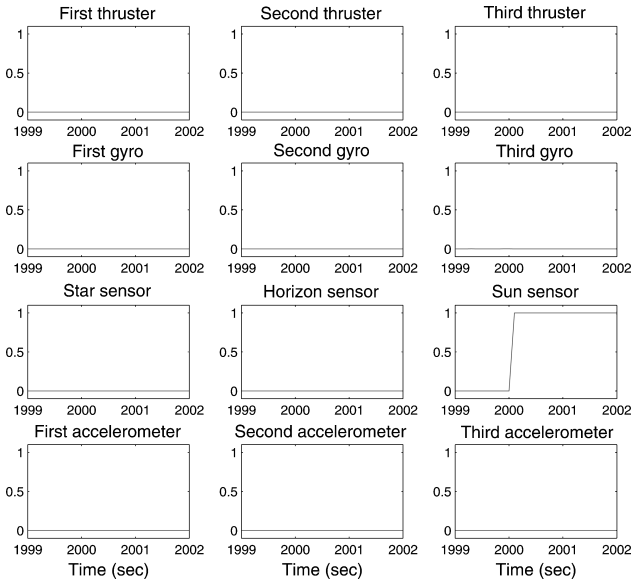

Fig. 13 Probabilities when sun sensor fault occurs.

sensor fault occurs, the residuals and probabilities are as shown in Figs. 10 and 11, respectively. When the sun sensor fault occurs, the residuals and probabilities are as shown in Figs. 12 and 13, respectively. Note that the norms of the projected residuals of the second periodic multiple-fault detection filter are scaled such that they become one when their associated target faults occur and when the satellite travels on the reference orbit without any disturbances and uncertainty. Figures 8, 10, and 12 show that when each of the star sensor, horizon sensor, and sun sensor-faults occurs, only the corresponding projected residual of the second multiple-fault detection filter becomes large while the other two projected residuals remain small. However, the projected residual that corresponds to the fault becomes small after a while even though the fault still exists. This is because the fault direction representing the fault magnitude is very small as discussed in Sec. V.A.2. Figures 9, 11, and 13 show that when each of the star sensor, horizon sensor, and sun sensor faults occurs, the residual processor announces the fault correctly in a fraction of a second.

VII. Conclusions

A health monitoring system based on analytical redundancy is developed for satellites on elliptical orbits. It consists of periodic-fault detection filters, parity equations, and residual processor. Its performance is evaluated in the simulation in the presence of disturbances and uncertainty. For the star sensor, horizon sensor, and sun sensor faults, the residual processor announces the fault in a fraction of a second. For the gyro faults, the residual processor announces the fault within $1\frac{1}{2}$ s. For the thruster and accelerometer faults, the residual processor announces the fault in about 4 s. If the fault magnitude is larger, the time that the residual processor needs to announce the fault will decrease. In the future, the health monitoring system will be evaluated in a more sophisticated simulation that considers drag, J2, and other perturbations.

Acknowledgment

This work was supported by NASA Goddard Space Flight Center under Grant NCC5-726.

References

[1]Massoumnia, M.-A., "A Geometric Approach to the Synthesis of Failure Detection Filters," *IEEE Transactions on Automatic Control*, Vol. AC-31, No. 9, 1986, pp. 839–846.

[2]Douglas, R. K., and Speyer, J. L., "Robust Fault Detection Filter Design," *Journal of Guidance, Control, and Dynamics*, Vol. 19, No. 1, 1996, pp. 214–218.

[3]Beard, R. V., "Failure Accomodation in Linear Systems through Self-Reorganization," Ph.D. Dissertation, Massachusetts Inst. of Technology, Cambridge, MA, Feb. 1971.

[4]Jones, H. L., "Failure Detection in Linear Systems," Ph.D. Dissertation, Massachusetts Inst. of Technology, Cambridge, MA, Aug. 1973.

[5]White, J. E., and Speyer, J. L., "Detection Filter Design: Spectral Theory and Algorithms," *IEEE Transactions on Automatic Control*, Vol. AC-32, No. 7, 1987, pp. 593–603.

[6]Douglas, R. K., and Speyer, J. L., "$\mathcal{H}_\infty$ Bounded Fault Detection Filter," *Journal of Guidance, Control, and Dynamics*, Vol. 22, No. 1, 1999, pp. 129–138.

[7]Massoumnia, M. A., and Verghese, G. C., and Willsky, A. S., "Failure Detection and Identification," *IEEE Transactions on Automatic Control*, Vol. AC-34, No. 3, 1989, pp. 316–321.

[8]Frank, P. M., "Fault Diagnosis in Dynamic Systems Using Analytical and Knowledge-based Redundancy—A Survey and Some New Results," *Automatica*, Vol. 26, No. 3, 1990, pp. 459–474.

[9]Patton, R. J., and Chen, J., "Robust Fault Detection of Jet Engine Sensor Systems Using Eigenstructure Assignment," *Journal of Guidance, Control, and Dynamics*, Vol. 15, No. 6, 1992, pp. 1491–1497.

[10]Chung, W. H., and Speyer, J. L., "A Game Theoretic Fault Detection Filter," *IEEE Transactions on Automatic Control*, Vol. AC-43, No. 2, 1998, pp. 143–161.

[11]Chen, R. H., and Speyer, J. L., "A Generalized Least-Squares Fault Detection Filter," *International Journal of Adaptive Control and Signal Processing—Special Issue: Fault Detection and Isolation*, Vol. 14, No. 7, 2000, pp. 747–757.

[12]Chen, R. H., Mingori, D. L., and Speyer, J. L., "Optimal Stochastic Fault Detection Filter," *Automatica*, Vol. 39, No. 3, 2003, pp. 377–390.

[13]Chen, R. H., and Speyer, J. L., "Robust Multiple-Fault Detection Filter," *International Journal of Robust and Nonlinear Control—Special Issue: Fault Detection and Isolation*, Vol. 12, No. 8, 2002, pp. 675–696.

[14]Malladi, D. P., and Speyer, J. L., "A Generalized Shiryayev Sequential Probability Ratio Test for Change Detection and Isolation," *IEEE Transactions on Automatic Control*, Vol. AC-44, No. 8, 1999, pp. 1522–1534.

[15]Bell, D. J., and Jacobson, D. H., *Singular Optimal Control Problems*, Academic Press, London, 1975.

[16]Moylan, P. J., and Moore, J. B., "Generalizations of Singular Optimal Control Theory," *Automatica*, Vol. 7, No. 5, 1971, pp. 591–598.

[17]Athans, M., "The Matrix Minimum Principle," *Information and Control*, Vol. 11, No. 5/6, 1968, pp. 592–606.

[18]Speyer, J. L., and White, J. E., "Shiryayev Sequential Probability Ratio Test for Redundancy Management," *Journal of Guidance, Control, and Dynamics*, Vol. 7, No. 5, 1984, pp. 588–595.

[19]Shiryayev, A. N., *Optimal Stopping Rules*, Springer-Verlag, New York, 1978, Chap. 4.

[20]Bittanti, S., Laub, A. J., and Willems, J. C., *The Riccati Equation*, Springer-Verlag, Berlin, 1991, Chap. 6.

[21]Shayman, M. A., "Phase Portrait of the Matrix Riccati Equation," *SIAM Journal on Control and Optimization*, Vol. 24, No. 1, 1986, pp. 1–65.

[22]Wertz, J. R., *Spacecraft Attitude Determination and Control*, Kluwer Academic, Dordrecht, The Netherlands, 1978, p. 29, Chaps. 5–7.

[23]Meyer, R. X., *Elements of Space Technology for Aerospace Engineers*, Academic Press, San Diego, CA, 1999, p. 233.

[24]*Global Positioning System: Papers Published in Navigation*, Vol. 5, Inst. of Navigation, Alexandria, VA, 1998.